

Nonlinear dynamics of a shear banding interface

S. M. Fielding*

*School of Mathematics, University of Manchester,
Booth Street East, Manchester M13 9EP, United Kingdom*

P. D. Olmsted

*Polymer IRC and School of Physics & Astronomy,
University of Leeds, Leeds LS2 9JT, United Kingdom*

(Dated: November 12, 2018)

We study numerically the nonlinear dynamics of a shear banding interface in two dimensional planar shear flow, within the non-local Johnson Segalman model. Consistent with a recent linear stability analysis, we find that an initially flat interface is unstable with respect to small undulations for sufficiently small ratio of the interfacial width ℓ to cell length L_x . The instability saturates in finite amplitude interfacial fluctuations. For decreasing ℓ/L_x these undergo a non equilibrium transition from simple travelling interfacial waves with constant average wall stress, to periodically rippling waves with a periodic stress response. When multiple shear bands are present we find erratic interfacial dynamics and a stress response suggesting low dimensional chaos.

PACS numbers: 47.50.+d, 47.20.-k, 36.20.-r.

Complex fluids such as polymers, liquid crystals and surfactant solutions have mesoscopic structure that is readily perturbed by flow [1]. For example, wormlike surfactant micelles with lengths of the order of microns can be induced to stretch, disentangle and entangle, and break or increase in length. Their mechanical response is therefore highly non-Newtonian, with shear flows inducing normal stresses (*e.g.* $\sigma_{xx} - \sigma_{yy}$), and with the shear stress σ_{xy} being a nonlinear function of applied shear rate $\dot{\gamma}$. Recent work on such fluids has led to a fairly consistent picture of “shear banding”: coexistence in shear flow of viscously thicker (nascent) and thinner (flow-induced) bands of material flowing at different local shear rates, for an overall average imposed shear rate.

This phenomenon can be described by constitutive models for which the shear stress is a non-monotonic function of shear rate for homogeneous flow. This leads to a separation into bands of differing shear rate that coexist at a common shear stress [2, 3]. Although most studies have assumed a flat interface between the bands and (with a few exceptions [4]) predicted a time-independent banded state, an accumulating body of data has demonstrated that the average shear stress, and the banding interface, can fluctuate [5, 6, 7, 8, 9, 10, 11, 19]. An important question is then whether these fluctuations resemble small amplitude capillary waves stabilised by surface tension, or whether they arise from an underlying instability, stabilised at large amplitude by nonlinearities. In this Letter we give strong evidence supporting the latter scenario, via the first theoretical study of the nonlinear dynamics of a shear banding interface.

The model – The generalised Navier Stokes equation for a viscoelastic material in a Newtonian solvent of viscosity η and density ρ is:

$$\rho(\partial_t + \mathbf{v} \cdot \nabla) \mathbf{v} = \nabla \cdot (\boldsymbol{\Sigma} + 2\eta \mathbf{D} - P\mathbf{I}), \quad (1)$$

where $\mathbf{v}(\mathbf{r})$ is the velocity field. The pressure P is deter-

mined by incompressibility, $\nabla \cdot \mathbf{v} = 0$. The viscoelastic stress $\boldsymbol{\Sigma}(\mathbf{r})$ evolves according to the non-local (“diffusive”) Johnson Segalman (DJS) model [12, 13]

$$\begin{aligned} & (\partial_t + \mathbf{v} \cdot \nabla) \boldsymbol{\Sigma} - a(\mathbf{D} \cdot \boldsymbol{\Sigma} + \boldsymbol{\Sigma} \cdot \mathbf{D}) \\ & - (\boldsymbol{\Sigma} \cdot \boldsymbol{\Omega} - \boldsymbol{\Omega} \cdot \boldsymbol{\Sigma}) = 2G\mathbf{D} - \frac{\boldsymbol{\Sigma}}{\tau} + \frac{\ell^2}{\tau} \nabla^2 \boldsymbol{\Sigma}, \end{aligned} \quad (2)$$

with plateau modulus G and relaxation time τ . \mathbf{D} and $\boldsymbol{\Omega}$ are the symmetric and antisymmetric parts of the velocity gradient tensor, $(\nabla \mathbf{v})_{\alpha\beta} \equiv \partial_\alpha v_\beta$. For $a = 1$ and $\ell = 0$ this model reduces to the Oldroyd B model, which is motivated by considering an ensemble of beads paired by springs (simplified polymer chains) into dumbbells. Stress is generated as the flow deforms the dumbbells, and is relaxed on the timescale τ for the springs to regain equilibrium length. To capture shear thinning the DJS model invokes a “slip parameter” a with $|a| < 1$ to give non-affine dumbbell deformation [12]. The constitutive curve $T_{xy} = \Sigma_{xy}(\dot{\gamma}, a) + \eta\dot{\gamma}$ for homogeneous planar shear $\mathbf{v} = y\dot{\gamma}\hat{\mathbf{x}}$ is then capable of non-monotonicity, allowing shear banding. The non-local diffusive term in Eqn. 2 accounts for spatial gradients across the banding interface on a length scale ℓ [13]. It arises naturally in models of liquid crystals, and diffusion of polymer molecules [14]. In the context of one dimensional (1D) calculations, it has been shown to give a unique (selected) stress T_{xy}^* at which banding occurs [13], as seen experimentally.

We study 2D boundary-driven flow between parallel plates at $y = 0, L$ with plate conditions $\partial_y \Sigma_{\alpha\beta} = 0 \forall \alpha, \beta$ for the viscoelastic stress, and no slip or permeation for the velocity. In the flow direction we consider a domain $x = \{0, L_x\}$, with periodic boundary conditions. We choose $a = 0.3, \eta = 0.05$ throughout, and units in which $G = 1, \tau = 1$ and $L = 1$.

For an imposed average shear rate $\bar{\gamma} \equiv [v_y(L) - v_y(0)]/L$ in the region of decreasing stress, $dT_{xy}/d\dot{\gamma} < 0$, homogeneous flow is unstable [15]. A 1D (y) calcula-

tion then predicts separation into bands of shear rates $\dot{\gamma}_1 = 0.66, \dot{\gamma}_2 = 7.09$, at a selected shear stress $T_{xy}^* = 0.506$. Recent analysis [16] showed this stationary 1D banded state to be linearly unstable to 2D (x, y) perturbations corresponding to undulations of the interface with wavevector $\mathbf{q} = q_x \hat{\mathbf{x}}$. The most unstable mode has $q_x L \approx 2\pi$, and the instability involves feedback of the normal stress with velocity fluctuations across the interface. In this Letter, we study the fate of the interface in the *nonlinear* regime, and demonstrate it to be restabilised at the level of finite amplitude undulations.

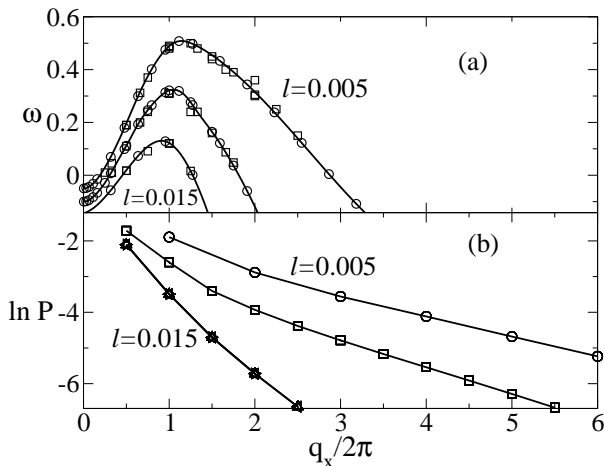


FIG. 1: (a) Growth rate $\omega(q_x)$ of perturbations about an initially 1D banded state. (\circ , —): predictions of linear stability [16] for $\ell = 0.005, 0.01, 0.015$. (\square): early time dynamics of the full 2D numerics for $\ell = 0.005, L_x = 4, 6, 8$; $\ell = 0.01, L_x = 2, 4, 6, 8$; $\ell = 0.015, L_x = 2, 4, 8$. (b) Power spectrum $P(q_x)$ in the travelling wave regime for $\ell = 0.005, L_x = 1$ (\circ); $\ell = 0.01, L_x = 2$ (\square); $\ell = 0.015, L_x = 2, 4, 6$ (\triangle).

Numerical scheme— We enforce incompressibility by eliminating the velocity in favour of a stream-function ψ . At each time step we update the local parts of Eqn. 2 using an explicit Euler algorithm within a finite difference scheme on a rectangular grid of (N_x, N_y) nodes, using third order upwinding for the convective term $(\mathbf{v} \cdot \nabla) \Sigma$. We then take a Fourier transform $x \rightarrow q_x$ in the flow direction and update the nonlocal part of Eqn. 2 using the semi-implicit Crank-Nicolson algorithm. We finally update Eqn. 1 at zero Reynolds number, $\rho = 0$. We attain convergence to one percent with respect to increasing spatial and temporal resolution. This ensures that the results shown are converged to the eye, apart from the stress signal $\bar{T}_{xy}(t)$ in Fig. 4: this shows slight quantitative, but not qualitative, changes. Runs at finer resolution are prohibitively time consuming. We study two initial conditions: (IC1) the stationary banded state, predicted by a 1D calculation, of two bands separated by flat interface; and (IC2) a homogeneous unstressed fluid, corresponding to shear startup from rest.

Linear regime— First we consider the early time evolution of an initially flat interface, IC1. For a wide enough interface ℓ and small enough system size L_x this 1D solu-

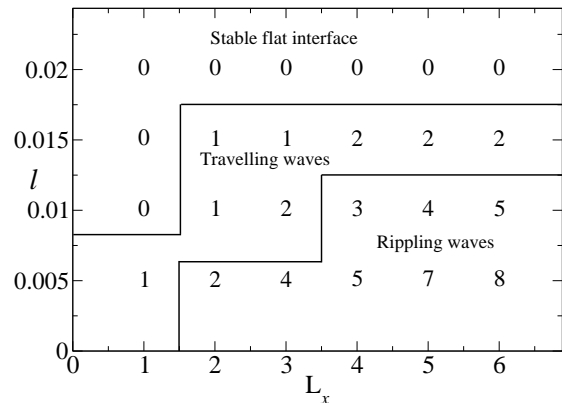


FIG. 2: “Phase diagram” for $\bar{\gamma} = 2.0$, showing the different non-linear regimes for IC1 (accurate to spacing between numbers) and the numbers of linearly unstable modes (Ref. [16]).

tion is stable. For smaller ℓ/L_x , however, interfacial undulations are predicted by the linear analysis of Refs. [16] to become unstable. Our numerics successfully reproduce this instability during the initial evolution away from IC1: the eigenvectors and growth rates $\omega(q_x)$ match the analytical results of Refs. [16], Fig 1. Beyond this early-time regime, the interface is restabilised by nonlinear effects, and the instability saturates in undulations of finite large amplitude. Depending on the distance from the onset of linear instability, Fig. 2, the ultimate attractor corresponds either to a steady travelling interfacial wave, or to periodically rippling waves.

Travelling wave— For values of ℓ/L_x marginally inside the unstable regime (Fig. 2) the ultimate attractor comprises a travelling wave $\mathbf{A} = \mathbf{A}(y, x - ct)$ for all order parameters $\mathbf{A} = \{\Sigma_{xx}, \Sigma_{xy}, \Sigma_{yy}, \psi\}$. Since this satisfies periodic boundary conditions, the wall-averaged shear stress is constant in time, with a value $\bar{T}_{xy,ss} \simeq 0.51 - 0.54$ that depends on ℓ and L_x and is slightly higher than the selected stress $T_{xy}^* = 0.506$ of the 1D calculation. In Fig. 3 the wave-speed $c = 1.15$, compared with a horizontal velocity v_x that varies between 1.439

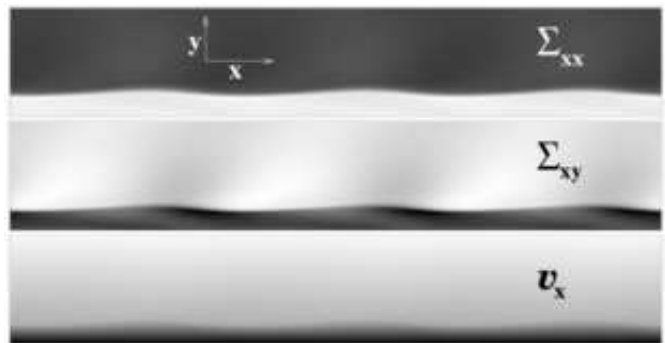


FIG. 3: Greyscale of order parameters for travelling wave in the (x, y) plane for $\ell = 0.015, L_x = 6$, and upper wall velocity $V \equiv \bar{\gamma}L = 2$ to the right.

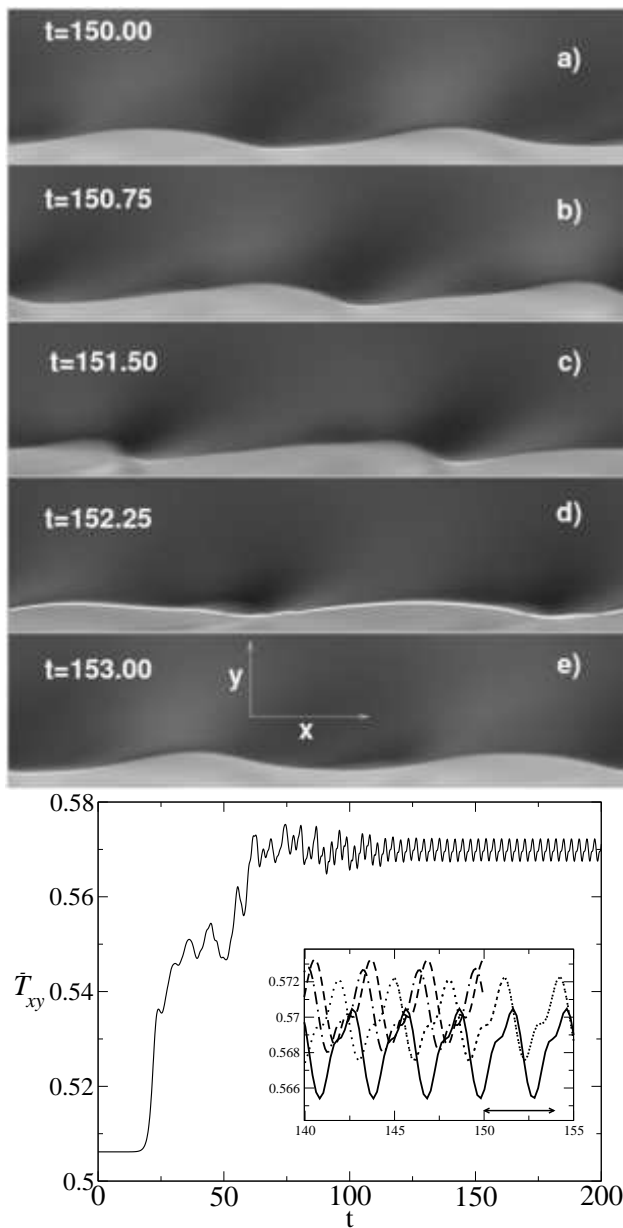


FIG. 4: Rippling wave at $\ell = 0.005$, $L_x = 4$, $\bar{\gamma} = 2$. Top: Greyscale of $\Sigma_{xx}(x, y)$. Upper wall moves to the right. White line in d): interface height defined in text. Bottom: average wall stress. Inset: $(N_x, N_y, dt) = (200, 800, 0.0003)$, solid line; $(400, 800, 0.0001)$, dotted; $(400, 800, 0.0003)$, dashed; $(500, 800, 0.0002)$, dot-dashed.

and 1.484 along the interface. To analyse the structure of this state we define the following power spectrum,

$$P(q_x) = \sum_{i=1}^4 \int_0^L dy |A_i(q_x, y)|^2. \quad (3)$$

As seen in Figs. 1 and 2, while the linear stability analysis predicted only a few unstable modes, the ultimate nonlinear state has active modes at higher q_x , Fig. 1b. Interestingly, the dominant mode is still close to that of

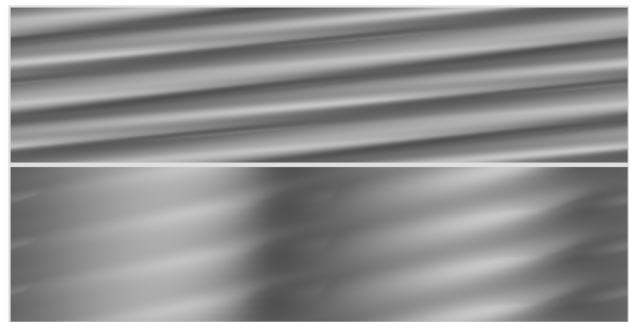


FIG. 5: Rippling wave regime. Greyscale of interface height (defined in text) in (x, t) plane. Parameters as in Fig. 4. Time $t = 150 \dots 160$ upwards. Upper: raw data. Lower: transformed as $x \rightarrow x - ct$, c extracted by eye.

the linear analysis, despite being in a nonlinear regime with a finite interfacial displacement δh . Indeed, for all cases in Fig. 1b, we find empirically that the dominant mode has the longest wavelength that is both consistent with periodic boundary conditions and linearly unstable.

Rippling wave— For smaller ℓ/L_x , deeper inside the unstable regime (Fig. 2), we see a new regime in which the travelling wave now periodically “ripples”. The wall-averaged stress \bar{T}_{xy} is periodic in time (Fig. 4, again for IC1), with variations of the order of one percent, and an average value larger than the 1D selected stress T_{xy}^* . The interface height $h(x)$ is shown as a white line in Fig. 4d and as a greyscale over a time window in Fig. 5. Because the structure is quite complicated near a rippling wave (Figs. 4cd), the location of $h(x)$ depends on its precise definition. We take $h(x)$ as that value of y at which Σ_{xx} lies half way between its values at the two walls. (An alternative might be $\int dy y |\partial_y \Sigma_{xx}(y)|$.) This provides a fairly reliable measure, subject to a small kink in the rippling region (Fig. 4d).

Robustness to initial conditions— So far, we have considered only IC1, two bands separated by a single flat interface. To test robustness to ICs, we now study startup from rest (IC2). Here the system develops either (i) two bands that show the same dynamics as with IC1, or (ii) multiple bands that have erratic dynamics suggestive of low dimensional chaos, Fig. 6. This is the counterpart of startup from rest in 1D planar shear flow, which typically yields random configurations of multiple bands, because the uniform shear stress $T_{xy}(y) = T_{xy}^*$ allows interfaces to reside at any y value. (To achieve IC1, the system was prebiased to form two bands.) In contrast, Couette flow between concentric cylinders has a stress $T_{xy} \sim 1/r^2$ (r =radius), which allows only a single stationary interface at $r^* \sim 1/\sqrt{T_{xy}^*}$, as demonstrated in 1D in Ref. [17, 18]. By analogy, we anticipate that curvature should eliminate the multiple band case (ii) in 2D. Although a true Couette calculation has not been performed, we implement a “poor man’s” version by adding a biasing stress-gradient in the y direction while the bands are forming. For strong enough bias, we then

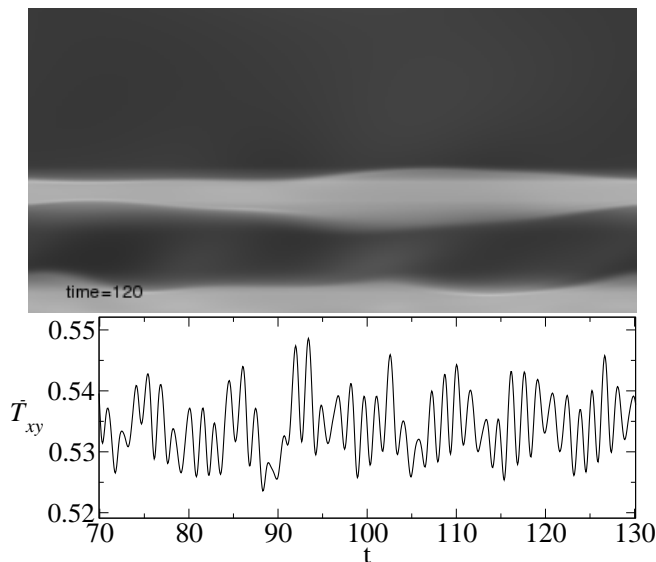


FIG. 6: Multiple bands after startup from rest for $\ell = 0.005$, $L_x = 2$, $\bar{\gamma} = 2$. Top: greyscale of $\Sigma_{xx}(x, y)$ at time $t = 120$, reconstructed from the first 15 Fourier modes. Bottom: Shear stress $T_{xy}(t)$.

indeed find case (i), just two bands. An open question is whether, even with IC1, a transition exists in the numerically inaccessible regime of small ℓ/L_x (far bottom right in Fig. 2) to chaotic dynamics of a single interface.

To summarise, we have studied numerically the nonlinear dynamics of a shear banding interface in 2D planar shear flow, within the non-local DJS model, for a system of length L_x with periodic boundary conditions in

x . Upon decreasing the ratio of the interfacial width ℓ to the system length L_x the stable two band state separated by a single interface undergoes successive transitions to travelling waves and rippling travelling waves. Multiple shear bands can also be found, depending on initial conditions, which show irregular interfacial dynamics and a corresponding stress signal suggestive of low dimensional chaos. Depending on the regime, this dynamics is qualitatively similar to several recent experiments in wormlike micellar solutions that studied the interfacial dynamics and the associated stress response [5, 6, 10, 19].

In earlier work, Yuan *et al.* [20] used a 2D finite element algorithm to evolve a related JS model in planar shear. Contrary to our results, they reported a stable interface. However, they considered rather small values of L_x , perhaps in the stable regime, and the finite element technique may have introduced stabilising numerical diffusion. Related recent work by Onuki [21] on a two-fluid version of the DJS model [22] at imposed stress also showed a variety of interesting time-dependent behaviour due to the interplay between stress and concentration degrees of freedom; it would be interesting to study the phenomena found here in that model. Indeed, an open question is the extent to which the instability seen in this DJS model is ubiquitous among other models of shear banding, such as those for liquid crystals. Future work should also extend to larger systems and smaller interfaces, likely to lead to more complex dynamical states.

SMF thanks Prof. Ajdari for his hospitality at the ESPCI in Paris where this work was partly carried out, and UK EPSRC GR/S29560/01 for financial support. We thank O. Harlen and H. Wilson for helpful discussions.

* Electronic address: suzanne.fielding@manchester.ac.uk

- [1] R. G. Larson, *The Structure and Rheology of Complex Fluids* (Oxford University Press, New York, 1999).
- [2] N. A. Spenley, M. E. Cates, and T. C. B. McLeish, *Phys. Rev. Lett.* **71**, 939 (1993).
- [3] P. D. Olmsted, *Curr. Op. Coll. Int. Sci.* **4**, 95 (1999).
- [4] S. M. Fielding and P. D. Olmsted, *Phys. Rev. Lett.* **92**, 084502 (2004); A. Aradian and M. E. Cates, *Europhys. Lett.* **70**, 397 (2005).
- [5] L. Becu, S. Manneville, and A. Colin, *Phys. Rev. Lett.* **93**, 018301 (2004).
- [6] M. R. Lopez-Gonzalez, W. M. Holmes, P. T. Callaghan, and P. J. Photinos, *Phys. Rev. Lett.* **93**, 268302 (2004).
- [7] A. S. Wunenburger, A. Colin, J. Leng, A. Arneodo, and D. Roux, *Phys. Rev. Lett.* **86**, 1374 (2001).
- [8] W. M. Holmes, M. R. Lopez-Gonzalez, and P. T. Callaghan, *Europhys. Lett.* **64**, 274 (2003).
- [9] Y. T. Hu, P. Boltenhagen, and D. J. Pine, *J. Rheol.* **42**, 1185 (1998).
- [10] E. K. Wheeler, P. Fischer, and G. G. Fuller, *J. Non-Newt. Fl. Mech.* **75**, 193 (1998).
- [11] S. Manneville, J. B. Salmon, L. Becu, A. Colin, and F. Molino, *Rheol. Acta* **43**, 408 (2004); J. B. Salmon, L. Becu, S. Manneville, and A. Colin, *Eur. Phys. J. E* **10**, 209 (2003).
- [12] M. Johnson and D. Segalman, *J. Non-Newt. Fl. Mech* **2**, 255 (1977).
- [13] P. D. Olmsted, O. Radulescu, and C.-Y. D. Lu, *J. Rheology* **44**, 257 (2000).
- [14] A. W. El-Kareh and L. G. Leal, *J. Non-Newt. Fl. Mech.* **33**, 257 (1989).
- [15] J. Yerushalmi, S. Katz, and R. Shinnar, *Chemical Engineering Science* **25**, 1891 (1970).
- [16] S. M. Fielding, *Phys. Rev. Lett.* **95**, 134501 (2005); H. J. Wilson and S. M. Fielding, submitted to *JNNFM*.
- [17] F. Greco and R. C. Ball, *J. Non-Newt. Fl. Mech.* **69**, 195 (1997).
- [18] O. Radulescu and P. D. Olmsted, *J. Non-Newt. Fl. Mech* **91**, 141 (2000).
- [19] R. Bandyopadhyay, G. Basappa, and A. K. Sood, *Phys. Rev. Lett.* **84**, 2022 (2000).
- [20] L. Jupp and X. F. Yuan, *J. Non-Newton. Fluid Mech.* **124**, 93 (2004); X. F. Yuan, *Europhys. Lett.* **46**, 542 (1999).
- [21] A. Furukawa and A. Onuki, *Physica D* **205**, 195 (2005).
- [22] S. M. Fielding and P. D. Olmsted, *Phys. Rev. Lett.* **90**, 224501 (2003).